Broadband ultrafast terahertz spectroscopy in the 25 T Split Florida-Helix

Jeremy A. Curtis, Ashlyn D. Burch ⓘD, Biplob Barman, A. Garrison Linn, Luke M. McClintock, Aidan L. O'Beirne, Matthew J. Stiles, John L. Reno, Stephen A. McGill, Denis Karaiskaj, and David J. Hilton ⓘD

View Online   Export Citation   CrossMark

ARTICLES YOU MAY BE INTERESTED IN

Broadband ultrafast terahertz spectroscopy in the 25 T Split Florida-Helix

Jeremy A. Curtis,[1,a)] Ashlyn D. Burch,[1,a)] Biplob Barman,[1] A. Garrison Linn,[1]
Luke M. McClintock,[1] Aidan L. O'Beirne,[1] Matthew J. Stiles,[1] John L. Reno,[2]
Stephen A. McGill,[3] Denis Karaiskaj,[4] and David J. Hilton[1,b)]

[1]*Department of Physics, University of Alabama at Birmingham, Birmingham, Alabama 35294, USA*
[2]*Center for Integrated Nanotechnologies, Sandia National Laboratories, Albuquerque, New Mexico 87185, USA*
[3]*National High Magnetic Field Laboratory, Florida State University, Tallahassee, Florida 32310, USA*
[4]*Department of Physics, University of South Florida, Tampa, Florida 33620, USA*

We describe the development of a broadband (0.3–10 THz) optical pump-terahertz probe spectrometer with an unprecedented combination of temporal resolution (≤200 fs) operating in external magnetic fields as high as 25 T using the new Split Florida-Helix magnet system. Using this new instrument, we measure the transient dynamics in a gallium arsenide four-quantum well sample after photoexcitation at 800 nm. *Published by AIP Publishing.* https://doi.org/10.1063/1.5023384

I. INTRODUCTION

Ultrafast spectroscopic techniques permit the study and control of the optical and electronic properties of materials on time scales faster than traditional electronic techniques can resolve. Currently available femtosecond lasers can produce ultrafast pulses over a wide range of the spectrum including ultraviolet,[1] optical,[2] infrared,[3] and/or terahertz.[4] In these experiments, a femtosecond pump pulse from an ultrafast laser perturbs the sample, while a time-delayed probe pulse studies the transient changes to the complex dielectric constants of materials. At low pump pulse energies, these experiments study the near-equilibrium properties of materials, while as the pulse energy is increased, these can be used to study strongly non-equilibrium dynamics,[5] metastable phases,[6] and photoinduced phase transitions.[7] Using ultrafast lasers to study and manipulate the optical properties of materials, for example, can trigger phase transitions to alternate orders that cannot be easily accessed using other experimental techniques, and thus, they can help elucidate the underlying competition between different degrees of freedom in a material.[5] Investigation of non-equilibrium dynamics and metastable phases generally requires control of these material properties on a pico- or femtosecond time scale. This enables the dynamic tuning of one degree of freedom (e.g., charge, lattice, orbital, and spin) on a time scale that is faster than it is coupled to the other degrees of freedom. This enables the system to move into an otherwise thermodynamically inaccessible metastable configuration.[7]

In this paper, we describe the development of our broadband optical pump-terahertz probe spectrometer that operates in *sustained* high magnetic fields. This uses the 25 Tesla Split Florida-Helix magnet at the National High Magnetic Field Lab, which has been designed with multiple optical axes for *free-space* optical experiments. We use this new spectrometer to study light-induced changes to the terahertz dielectric

constants in a 18 nm semiconductor multiple quantum well (VA0719). An excitation pulse excites the 18 nm multiple quantum well sample using the output ($h\nu_1$ = 1.55 eV) of a mode-locked titanium:sapphire laser amplifier, while the probe measures the changes to the sample transmission using a time-delayed broadband terahertz pulse derived from the same laser amplifier. We observe a reduction in the transmitted terahertz bandwidth when compared to the generated pulse that is consistent with the reststrahlen bands of gallium arsenide and aluminum gallium arsenide in the quantum well. Finally, we discuss the broader applicability of our new instrument to a wider range of material systems, including the complex and competing dynamics between electronic, orbital, lattice, and spin degrees of freedom in many correlated electron systems.

II. ULTRAFAST SPECTROSCOPY IN CORRELATED SYSTEMS AND QUANTUM-CONFINED SEMICONDUCTORS

Spin has an important role in the electronic and magnetic phases of many materials including common semiconductors,[8–11] transition metal oxides (e.g., manganites,[12,13] cuprates,[14,15] nickelates,[16] iridates,[17,18] and vanadates[19]), transition metal dichalcogenides,[20] and pnictides.[21] External control of spin in these systems either requires the use of light[22] through spin-orbit coupling in the material or external magnetic fields, which split spin states into different energy levels.[13] An improved understanding of the underlying physics responsible for these metastable phases will be aided by a new generation of ultrafast experimental tools that can measure and control the electronic, lattice, orbital, and/or spin degrees of freedom.

The utility of our instrument is its ability to study the collective and single-particle excitations within a wide range of materials of contemporary interest. Figure 1 highlights some of these excitations, which are present in a wide variety of two-dimensional materials, correlated electron materials, and

a)J. A. Curtis and A. D. Burch contributed equally to this work.
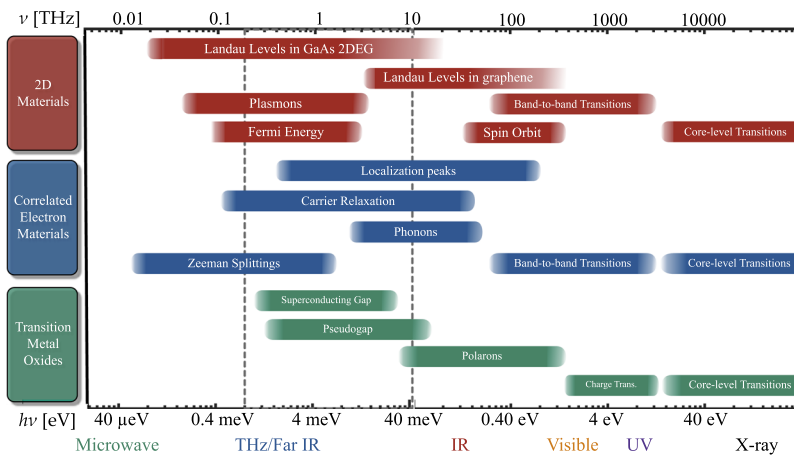b)dhilton@uab.edu

FIG. 1. This figure highlights a subset of quasiparticles that are of interest in condensed matter, including two-dimensional materials, correlated electron materials, and transition metal oxides. The boxed frequency range (0.3 THz–10 THz, gray box) is that of the probe pulse that is described in this manuscript. A broader listing of relevant low energy excitations in a wider variety of condensed matter materials can be found in Fig. 3 of Ref. 14.

transition metal oxides. Doped and undoped quantum wells have been extensively studied using traditional electrical techniques,[23–25] microwave spectroscopy,[26] and more recently terahertz time-domain techniques,[27–29] revealing this rich and complex phase diagram as a function of the external magnetic field applied both parallel (defined to be B_y in this manuscript) and perpendicular (defined to be B_z in this manuscript) to the quantum wells. High quality two-dimensional samples of gallium arsenide show Landau levels that can be explained using a model of weakly interacting quasiparticles in an external magnetic field.[30] Under *high* magnetic field and at low temperatures, however, a number of more exotic electronic phases emerge that result from strong interactions[31,32] or modifications to the Fermi surface.[33] Amongst more exotic materials, the enhancement of superconductivity in two-dimensional superconductors (e.g., the $LaAlO_3$–$SrTiO_3$ interface) by the application of parallel magnetic field has been attributed to the paramagnetic impurities that, in part, suppress superconductivity in these materials.[34] In colossal magnetoresistive manganites (e.g., $La_{1-x}Ca_xMnO_3$), the resulting ultrafast dynamics can be described by a two-component decay that is determined by thermally disordered phonons and spin fluctuations in different temperature and field ranges.[35]

III. BACKGROUND

Ultrafast pump-probe spectroscopy uses femtosecond lasers to perturb a sample from equilibrium as well as to probe the transient optical properties.[30] Ultrafast magnetospectroscopy experiments add an external magnetic field to elucidate the influence that spin has on the optical and electronic properties of materials. For magnetic fields less than 10 T, split-coil magnets are commercially available and use a pair of superconducting coils on either side of the sample space to generate the external magnetic field. These have an available optical axis with a sizable numerical aperture and allow the use of experiments that generate and collect the transmitted/reflected light using free space propagation techniques.[28,29,36]

Bitter magnets are a resistive magnet design and are capable of much higher magnetic field generation. These are constructed using an interlocking stack of helical copper disks that circulate large currents around a small central opening

where a sample is located. Since the magnet is usually several meters in length to create a uniform high magnetic field at the sample space, this geometry has a small numerical aperture available along the optical axis to probe a sample in the high magnetic field.[37] As a consequence of their geometry, Bitter magnets usually require the use of optical fibers to couple light sources and detectors into and out of the magnetic field.[30,38] Light from an external source is coupled into an optical fiber and the reflected or transmitted light is collected in an optical fiber to return to an external detector/spectrometer for measurement.[39]

A fiber-coupled Bitter magnet experiment is suitable for continuous wave visible and near-infrared photoluminescence experiments, for example, where there are suitable light sources, detectors/spectrometers, and optical fibers.[39,40] It is much more challenging for time-resolved experiments that use broadband pulsed lasers or that operate at terahertz frequencies.[41] Dispersion and higher order nonlinearities (e.g., Brillouin scattering and self-phase modulation) of optical fibers make their use in femtosecond pulse experiments, at best, complicated.[38,42]

The study of metastable phases of matter would require high fluence excitation where the use of fiber optics is even more problematic. Titanium:sapphire lasers/laser amplifiers have pulse energies ranging from a few nanojoules to multiple millijoules.[2] At low pulse energies, fiber propagation of femtosecond pulses requires compensation for both group velocity dispersion and nonlinear optical effects such as self-phase modulation, for example, which can make propagation of ≤100 fs pulses difficult or impossible.[38] For high pulse energies that are near to or exceed the damage threshold of the optical fiber, alternate techniques are needed to adapt ultrafast spectroscopic measurements to high B field magnets because of a wide range of novel experiments that could be of interest in this strongly non-equilibrium regime.

We focus our development efforts on *time-resolved* experimental techniques that can provide information on the non-equilibrium evolution of the terahertz frequency complex dielectric constants with sub-picosecond temporal resolution. Alternate methods include a number of lasers, glow bars, backward wave oscillators, quantum cascade lasers, and free electron lasers, among many other sources used to generate light from 0.3 to 10 THz.[43,44] These light sources can be

coupled into high field magnets using a variety of light pipe configurations and have been previously used to study the near-equilibrium dielectric properties of a series of multiferroic materials.[45–47]

The recent development of a compact pulsed magnet with a 30 T *peak* magnetic field is notable for its high numerical aperture optical axis that is suitable for many conventional ultrafast experiments. This has been used to demonstrate terahertz time-domain spectroscopy via rapid scan optics to reconstruct the terahertz electric field.[48,49] The small number of shots per day for this magnet, however, makes this technique appropriate for experiments that require a limited number of data points.

The major technological advance to enable our new broadband ultrafast spectrometer is the recently commissioned Split Florida-Helix magnet system at the National High Magnetic Field Lab, which is capable of sustained operation at fields as high as $B_y = 25$ T.[50] The electrical power consumption of this *resistive* magnet is 32 MWh, but the ability to maintain a DC high magnetic field enables a different set of experiments than would be possible with pulsed magnet systems.

Our instrument will employ a conventional broadband terahertz spectrometer[51] that has been adapted to operate in the Split Florida-Helix magnet in free space operation, which requires the large numerical aperture optical axis commonly seen in split-coil magnets. The Split Florida-Helix has been specifically constructed with wide-angle optical access to the high peak field region. This is an adaptation of the standard Bitter resistive magnet design that has an additional mid-plane assembly with optical windows to allow for light to propagate through the sample region at $B_y = 25$ T.[52] As a result, the Split Florida-Helix has a numerical aperture of $45° \times 12°$ that allows for collection of the transmitted, reflected, or scattered light.[30] The light generation and detection occur entirely *outside* of the magnet, eliminating many of the complications of optical fibers and reducing the effect that the magnet has on both the light generation mechanisms as well as the electronics in the detector.

IV. INSTRUMENT DESIGN AND COMPONENTS

A. Design goals

We have four main design goals for this instrument:

1. **High magnetic field operation**: The Split Florida-Helix magnet can sustain magnetic fields as high as $B_y = 25$ T. Our instrument operates in the Voigt geometry where the direction of light propagation ($\vec{k}$) is perpendicular to the magnetic field vector ($\vec{B}$). Faraday geometry ($\vec{k} \parallel \vec{B}$) is also possible with this experiment, but this requires modifications to the magnet that are beyond the scope of this manuscript.

2. **Broadband terahertz characterization**: We use a terahertz generation method that produces a pulse with frequency content from $\nu = 0.3$ to 10 THz and can directly study low energy excitations in materials over an energy range from $h\nu = 0.8$ to 41.4 meV ($h\nu = 6.7$ –333 cm^{-1}). For example, the superconducting gap and/or pseudogap in many common high temperature

superconductors occur within the temperature and magnetic field range of the instrument demonstrated in this manuscript. With the broadband terahertz pulse demonstrated here, the cyclotron energies of many common semiconductors[28] and two-dimensional materials[53] also lie within this energy range. A much more complete listing of relevant low energy excitations in a wide variety of condensed matter materials can be found in Fig. 3 of Ref. 14.

3. **Pump-probe configuration**: The output of the titanium:sapphire laser amplifier (Coherent, Legend Elite USX) is split into multiple beams to photoexcite the sample at 800 nm and to probe the resulting changes with a time-delayed broadband terahertz pulse. This takes advantage of the unique ability of the Split Florida-Helix to *sustain* a high magnetic field, as the full ultrafast pump-probe dynamics requires multiple experiments at a set of τ's to reconstruct the ultrafast dynamics.

4. **Cryogenic sample temperature**: The Split Florida-Helix has a 39 mm bore that uses a custom-constructed cryostat with a current base temperature of 15 K. The windows on the cryostat and the Split Florida-Helix magnet are fully replaceable; our experiment uses TPX™ (polymethylpentene) windows (Tydex, TPX window ⌀63.5 mm × 4.55 mm) that are transparent both at 800 nm as well as over the full probe pulse bandwidth (0.3–10 THz).

B. Titanium:sapphire laser amplifier

The laser system used in this experiment is a Coherent Legend Elite femtosecond laser amplifier that generates 25 fs pulses with a maximum pulse energy of $\mathcal{U} = 5$ mJ and a center wavelength of $\lambda_r = 800$ nm ($h\nu = 1.55$ eV) with a transform-limited bandwidth of $\Delta h\nu = 64$ meV (16 THz). Our magnetospectrometer uses recent advances in both broadband terahertz generation and detection methods[51,54,55] to produce terahertz pulses with a bandwidth from $\nu = 0.3$ THz to 10 THz. Figure 2 shows a schematic diagram of the terahertz spectrometer developed for the Split Florida-Helix magnet system. The amplifier output is split into three beams: the first is used to generate broadband terahertz pulses in a plasma filament, while the second is used to detect the transmitted terahertz pulses in a Terahertz-Air Breakdown Coherent Detector (THz-ABCD) detector (described below). The third beam is used to photoexcite the sample from equilibrium in an optical pump-terahertz probe configuration. The delay between the pump and the terahertz probe pulses is controlled by a mechanical delay stage (τ), while the detection of the transmitted terahertz field is recovered using the gate beam and a second mechanical delay stage to vary the difference (d) between the two beam paths.[56]

C. Generating broadband terahertz pulses

Terahertz generation mechanisms that use the air-plasma generation mechanism have been shown to produce *broadband* emission that extends to higher frequencies (0.3–10 THz in this manuscript) and with pulse energies as high as 1 μJ per pulse.[51,54,55] A near-infrared femtosecond pulse with a center
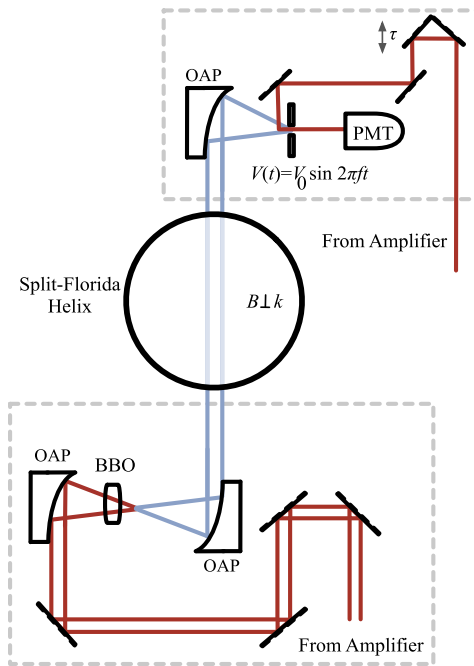
FIG. 2. The system generates broadband terahertz pulses by focusing a $\mathcal{U}_1 = 2.8$ mJ near-infrared pulse of an amplified titanium:sapphire laser in a nitrogen-purged atmosphere using an off-axis parabolic (OAP) mirror. Prior to the focus, a β-barium borate (BBO) crystal frequency doubles the 800 nm pulse, which generates broadband terahertz pulses from the dipole formed from the interference between single-photon (400 nm) and two-photon (800 nm) absorption in nitrogen.[51] The terahertz pulse is collimated using a second off-axis parabolic mirror and is transmitted through the sample in the Split Florida-Helix outfitted with a pair of TPX windows. The transmitted terahertz pulse is collected by a third off-axis parabolic mirror and focused into a Terahertz-Air Breakdown Coherent Detector (THz-ABCD). A portion ($\mathcal{U}_2 = 1$ mJ) of the titanium:sapphire beam is split from the generation arm and used to gate the THz-ABCD to recover the full electric field, $E(t)$. The titanium:sappire beam is also split into a pump beam ($\mathcal{U}_3 = 1.2$ mJ), delayed in time from the terahertz pulse (τ), and used to perturb the sample from equilibrium in an optical pump-terahertz probe configuration. The entire terahertz beam path is nitrogen purged to reduce the effects of water vapor absorption on our terahertz pulse.

wavelength of $\lambda_r = 800$ nm and a pulse energy of $\mathcal{U}_1 = 2.8$ mJ is focused in nitrogen and generates a plasma in the region of peak intensity. A β-barium borate (BBO) single crystal generates the second harmonic of the titanium:sapphire pulse at $\lambda_b = 400$ nm. Both pulses are focused in the plasma and a broadband terahertz pulse results from the interference between single-photon absorption of λ_b and two-photon absorption of λ_r.[51] Figure 3(a) shows the electric field of the generated terahertz pulse after transmission through the Split Florida-Helix magnet and the calculated broadband spectrum [Fig. 3(b)] with a usable bandwidth from 0.3 to 10 THz. This figure shows a continuous wavelet transform of the measured terahertz pulse and shows both the broad bandwidth as well as the short duration of this pulse, which is near the transform limit. The dashed line indicates the region above which the wavelet transform results are not affected by edge effects from the finite duration of the experimental data. This pulse was measured with the entire experiment assembled using the TPX windows but without a sample in place and demonstrates the maximum bandwidth possible in our current configuration. As we will show below, the actual bandwidth of any experiment conducted will also be

determined by the transmission of the sample/substrate. The entire terahertz path is purged with dry nitrogen to reduce the effects of water vapor absorption in the atmosphere.[57]

D. Detection of broadband terahertz pulses

Detection of the transmitted terahertz pulses in this experiment uses a Terahertz-Air Breakdown Coherent Detector (Zomega, ZAP-APD) to recover one linearly polarized component, $E_j(t)$, of the full terahertz electric field vector, $\vec{E}(t)$. A synchronized 3 kV power supply is modulated at half the repetition rate (500 Hz in this experiment) of the titanium sapphire laser amplifier and is applied to a pair of copper electrodes separated by an ~1 mm gap. A time-delayed gate pulse at $\lambda_r = 800$ nm is focused into this capacitor gap, and its second harmonic at $\lambda_b = 400$ nm is detected using a wavelength filter and a photomultiplier tube (PMT) detector.

In the absence of external voltage, air is a centrosymmetric medium that will not efficiently generate the second harmonic of the 800 nm detector gate pulse. The applied electric field generated in the gap breaks this symmetry and results in enhancement of the second harmonic generation and a concomitant increase in the second harmonic (400 nm) of the gate pulse. The external terahertz field is simultaneously focused into this gap, and the electric field of the component of the terahertz pulse along the direction of the bias electric field perturbs the second harmonic generation efficiency. The full terahertz electric field in the time-domain, $E(t)$, can be recovered by varying the delay (t) between the terahertz and the gate pulses and measuring the second harmonic.[56]

E. Waveform sampling and reconstruction

Each data point in an ultrafast pump-probe scan or terahertz waveform is a separate experiment at a fixed path length difference, d, between the pulses. The full ultrafast dynamics are acquired by repeating the experiment multiple times, while changing this path length difference (d_j) for each delay time (t_j), which makes this a time-consuming process. Measurement of the full terahertz time-domain waveform, $E(t)$, occurs over a finite window in time (T) and at a discrete set of points separated by a time difference $\Delta t = t_j - t_{j-1}$; the *measured* electric field, $E_s(t_j)$, can be used to reconstruct the full $E(t)$ with the correct set of t_j, while minimizing acquisition time because of the high energy usage of this resistive magnet. This measured electric field can be used to calculate the amplitude and phase of the complex spectrum, $\tilde{E}(\nu_j)$, using the Fourier transform and its inverse,

$$\text{FT}[f(t)] = \int_{-\infty}^{\infty} f(t) \exp(+i2\pi\nu t)dt, \quad (1a)$$

$$\text{IFT}\left[\tilde{F}(\nu)\right] = \int_{-\infty}^{\infty} \tilde{F}(\nu) \exp(-i2\pi\nu t)d\nu. \quad (1b)$$

Taking the numerical Fourier transform of the measured set of electric field points results in a complex spectrum given by the following equation:

$$\tilde{E}_s(\nu) = \sum_{m=-\infty}^{+\infty} \tilde{E}\left(\nu - \frac{m}{\Delta t}\right). \quad (2)$$
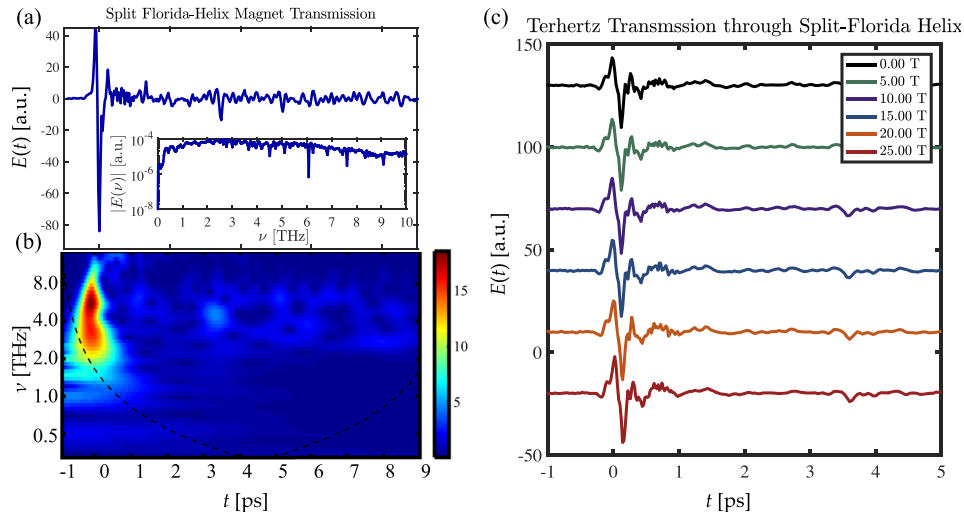
FIG. 3. (a) is a terahertz waveform, $E(t)$, after transmission through the experimental apparatus described in the text. This includes the TPX windows but with an empty sample position in the Split Florida-Helix magnet. Addition of the sample will reduce the bandwidth due to the reststrahlen bands in the substrate. The entire experiment was performed in a dry nitrogen atmosphere to minimize the absorption of atmospheric polar molecules (i.e., water, etc.). The inset plots the magnitude of the numerical Fourier transform, $|E(\nu)|$, on a logarithmic scale of the pulse shown in this panel, demonstrating the usable spectral bandwidth of 0.3–10 THz, over which the spectrum does not vary by more than one order of magnitude. The magnitude of the spectrum at 10 THz is approximately 6-7× smaller than that at the peak frequency, $\nu_{max} = 2.5$ THz. (b) shows the calculated spectrum of the terahertz pulse as a function of time. This is calculated using a symmetric Morse wavelet decomposition in MATLAB. This wavelet transform shows the spectral content as a function of time that is near the transform limit with a usable bandwidth from 0.3 to 10 THz. The dashed line indicates the region above which the wavelet transform results are not affected by edge effects from the finite duration of the experimental data. (c) To quantify the stability of this system, this figure shows a series of vertically offset terahertz waveforms taken with this experimental apparatus. These were acquired in the same configuration as (a) as a function of the magnetic field ($B_y = 0$–25 T) through the Split Florida-Helix with the TPX windows in place, but in the absence of any sample. The shift in the peak delay is less than $\Delta t \leq 40$ fs, which is 2× the sampling period in these data. Because of the sampling technique used to reconstruct the terahertz waveform, each terahertz waveform in this figure required approximately 20 min of magnet time to recover the electric field.

This contains both the desired complex spectrum ($m = 0$) as well as a series of frequency-shifted duplicates at multiples of the sampling rate, $m \times \Delta t^{-1}$. The Whittaker-Shannon sampling theorem directly relates the maximum frequency, $\nu_{max} \leq 2(\Delta t)^{-1}$, present in the terahertz waveform to the minimum required time-domain spacing, Δt.[58] With this criterion satisfied, the higher order duplicates of the spectrum (i.e., $m \neq 0$ in the summation) are isolated in frequency space from the fundamental ($m = 0$) and can be recovered using a numerical notch to produce the original spectrum, $\tilde{E}(\nu)$, and its inverse Fourier transform, $E(t)$. In the case of the present apparatus, the upper cutoff frequency is $\nu_{max} = 10$ THz in the absence of any sample in the Split Florida-Helix. This is determined by both the generation gas chosen (nitrogen) and the time-domain sampling ($\Delta t \leq 20$ fs) to maximize the spectrum acquired and minimize acquisition time.[59] Because the spectrum in our experiment is not well defined by an abrupt cutoff, oversampling ensures that the higher orders ($m > 0$) do not overlap with our fundamental ($m = 0$). The smaller step size would, however, increase the acquisition time that we would need to sustain magnetic fields and increase the electrical power consumption, so this oversampling must be minimized.

F. Long-range propagation of terahertz

Terahertz spectrometers have traditionally been compact devices due to the strong absorption of atmospheric water vapor in this frequency range.[60] This is also because of the difficulties inherent in collimating terahertz waves due to the

spatial diffraction of these long wavelengths.[49] The physical size of the Split Florida-Helix, with a diameter of ~2 m, *requires* long-distance propagation of terahertz light as it has the generation and detection components on opposite sides of the magnet. Our terahertz spectrometer can function over these long distances due to the high brightness of the generation mechanism as well as broadband operation, which has an enhanced high frequency content that is more easily collimated.

Diffraction losses preferentially affect lower frequencies when the optical components have spatial dimensions comparable to the wavelength ($\nu = 1$ THz corresponds to $\lambda \approx 300$ μm). At 1 THz, for example, $\lambda = 300$ μm would be diffracted more efficiently by the 1 cm sample aperture in the bore of the magnet than the upper frequency limit of our pulse (10 THz or $\lambda = 30$ μm). To account for any possible changes to the bandwidth of the terahertz pulse because of the magnet geometry,[61] we compare the spectrum at $B_y = 0$ to the spectrum at finite B_y in all of our calculations.[62]

G. System power estimates

This generation mechanism produces pulses with 0.2 μJ of energy per pulse (5.7×10^3 V cm^{-1}) with a beam that is spatially larger (~5 cm) than the available aperture through the magnet (~1 cm), so we expect that the pulse energy *at the sample position* is much lower due to clipping of the terahertz beam. This results in the reduction by one to two orders of magnitude after transmission through the limited aperture of the Split Florida-Helix. We are unable to directly measure the

strength of the terahertz field using our pyroelectric detector, which is larger than the available space; we have, however, verified that our experimental results are below the onset of nonlinear terahertz absorption features that occurred above $|\vec{E}| = 0.7$ kV cm^{-1} in Ref. 63; thus, we conclude that the peak field at the sample position is less than this value, but we will need further experiments to better calibrate this instrument's peak field *at the sample position*. The data shown in Fig. 3 demonstrate, however, a high signal-to-noise ratio even given these losses.

H. Long-term stability of the experiment

If the laser system alignment changes during an experiment, then changes to the terahertz spectrum could be the result of changes to the material properties or the change in the system alignment. Changes to the physical alignment of any metal optics or mounts may happen as the magnetic field is increased due to the force that results from their non-zero magnetic susceptibility. Also, system optics could have non-zero Veret constants that would demonstrate optical activity as a function of magnetic field. To quantify this *physical stability* of our experiment, we have measured the full terahertz waveform transmitted through the Split Florida-Helix as a function of the magnetic field in the absence of a sample but with all other optics/windows in place. Any change in the terahertz waveform, bandwidth, pulse timing, or amplitude would result from changes to the system alignment as a function of field or by residual magnetization in the optical components of our apparatus. Figure 3(c) shows terahertz waveforms transmitted through the Split Florida-Helix as a function of the magnetic field, showing a high degree of stability for the system over the ~60 min of acquisition time needed to acquire these data. The lower and upper frequencies are stable in these data to within ≤2% over the full magnetic field range, while the frequency dependent amplitude and phase are consistent, as well. The time delay of peak amplitude in each waveform varies by ≲40 fs from 0 to 25 T (sampling resolution of $\Delta t = 20$ fs), while the value of peak amplitude varies less than 5% in all data that are shown here. We can determine the uncertainty in measurements through samples with this knowledge of the systematic variation in our experimental alignment.

V. RESULTS

We demonstrate our spectrometer by measuring the light-induced changes to the terahertz frequency dielectric constants in a gallium arsenide multiple quantum well sample (VA0719). This heterostructure is grown on an undoped 625 μm (100) gallium arsenide substrate (AXT, Inc.) using molecular beam epitaxy. It has four doped 18 nm multiple quantum wells that have been δ-doped with Si at setback distances of 75 nm and 95 nm, resulting in a sheet carrier concentration of $n_s = 2 \times 10^{11}$ cm^{-2} in each well; we define the x–y plane to be the plane of the quantum wells, while the growth direction is defined to be the z direction. The separation of these individual quantum wells reduces the coupling of many-body excitations (i.e., indirect excitons, etc.) between wells and results, to first order, in the terahertz frequency dependent dielectric constants that are more characteristic of independent single quantum

wells.[64] Nonetheless, the contribution due to inter-well tunneling in these is not zero, as our results in this manuscript will demonstrate.[65]

To measure the light-induced change to the terahertz frequency properties of this sample, an optical pulse photoexcites the multiple quantum well with an above the bandgap pulse and probes the photoinduced change to the transmitted terahertz pulse, $\Delta E_s(t)$, as a function of the pump-probe delay (τ) for a range of external magnetic fields, B_y. Figure 4(a) shows the broadband terahertz pulse after transmission through this sample along with its time-frequency distribution for comparison with the terahertz pulse through the magnet only. The changes in both bandwidth and pulse duration in Fig. 3(a) are directly related to the constituent material's dielectric constants within the 0.3–10 THz frequency range. First, the *input* pulse has substantial frequency content beyond ~6.25 THz, which is not measured after transmission through the sample. Second, the pulse is near a single cycle in Fig. 3(a). After transmission through this sample, however, the pulse is spectrally chirped with higher frequencies that arrive with an additional phase shift relative to the input spectrum.

The limited bandwidth after transmission is consistent with resonant absorption in the sample, while the chirped phase near this absorption edge is consistent with the concomitant changes to the refractive index near a resonant frequency. Polar materials have reststrahlen bands where the resonant excitation of transverse optical (TO) phonons efficiently couple to the incident electromagnetic wave and prevent transmission through the sample. This results in strong *reflection* of the incident field back toward its initial source within a frequency range between the TO, ν_{TO}, and longitudinal optical (LO) phonon frequency, ν_{LO}. Within the terahertz band for one of these layers, the complex dielectric constant, $\tilde{\epsilon}(\nu)$, is given in the following equation:

$$\tilde{\epsilon}(\nu) = \epsilon_\infty + \sum_{j=1}^{N} \frac{f_j \nu_j^2}{\nu_j^2 - i\gamma_j \nu_j - \nu^2}, \qquad (3)$$

where f_j is the oscillator strength, ϵ_∞ is the high frequency dielectric constant, and ν_j is the set of transverse optical (TO) phonon frequencies and corresponding damping constants, γ_j. There exists a range of frequencies, $\nu_{TO} \leq \nu \leq \nu_{LO}$, where electromagnetic waves will not propagate through the sample since the real part of this dielectric constant is negative.[66] These lead to a substantial reduction in the transmitted signal through our 2DEG sample above $\nu \gtrsim 6.25$ THz due to the reststrahlen bands of GaAs as well those of Al$_x$Ga$_{1-x}$As used in the construction of this sample. We note that the restrictions from reststrahlen band transmission are common issues within this frequency range and need to be mitigated in future experiments by the choice of optical components and samples/substrates.[67]

Figure 4(b) shows optical pump terahertz probe data taken at $T = 20$ K as a function of the magnetic field from 0 to 20 T as a function of the pump-probe delay (τ) at a fixed gate delay (t).[68] These data show the dynamics of the change to the terahertz field peak amplitude that results from the above the bandgap optical pulse. These show a pulse-width limited decrease in terahertz peak electric field that is followed by a
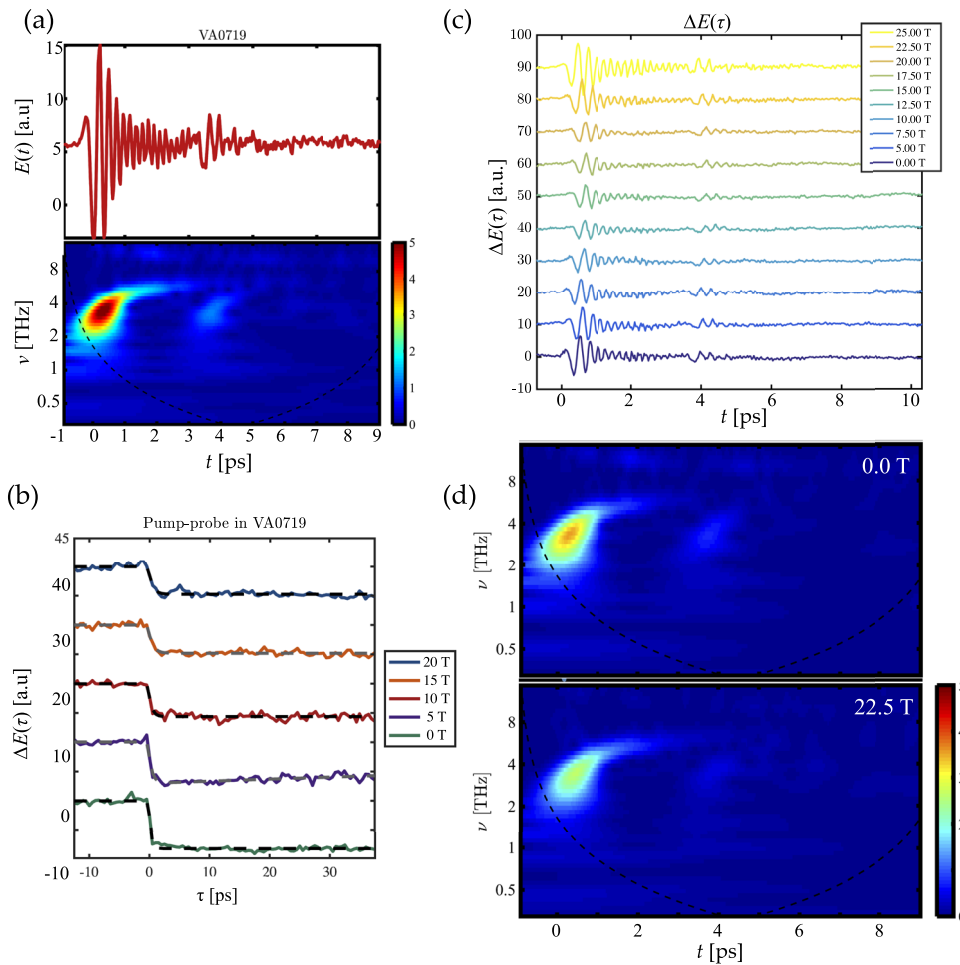
FIG. 4. (a) Terahertz waveform at 25 T taken in the pump-probe experiment in the multiple quantum well sample is shown here. Also shown here is the wavelet transform, showing the reduced bandwidth and chirped pulse spectra of the transmitted probe pulse due to the dispersive reststrahlen band of the gallium arsenide-based sample. (b) This figure shows a series of vertically offset optical pump terahertz probe traces taken with this experimental apparatus. Data for $\tau \leq 0$ are zero before the offset is applied. The optical pump terahertz probe data are taken in VA0719, where the solid lines are the experimental data taken when the gate (t) is aligned to the peak of the terahertz pulse and the dashed lines are a fit to Eq. (4). (c) The pump pulse induces a change to the terahertz waveforms, which we acquire as a function of magnetic field, B_y, and waveform delay, t. These data have a narrower bandwidth than the data shown in Fig. 3(c) due to the limited transmission of the substrate, as discussed in the text. (d) The wavelet transform is plotted at both $B_y = 0$ T and $B_y = 22.5$ T, which show similar bandwidth dynamics and demonstrating a strong spectral content above approximately 1.0 THz until 6.25 THz.

several hundred picosecond (or greater) recovery. We fit these data to a multi-exponential decay and recovery model given by Eq. (4), where $\vartheta(\tau)$ is the step function, τ_A is the initial life time over which the transmission changes, and τ_1 is the recovery time,

$$\Delta E(\tau) = A\vartheta(\tau)\left[1 - \exp\left(\frac{-\tau}{\tau_A}\right)\right]\exp\left(\frac{-\tau}{\tau_1}\right). \qquad (4)$$

These dynamics and the interpretation provided for them assumes that the photoinduced change to the sample transmission is dispersionless over the bandwidth of the terahertz pulse. In each of the fits, τ_A is pulse width limited, while the recovery time, τ_1, is much longer than the window that we have acquired data. While this is the case in these data, other material systems will have specific low-energy excitations within the bandwidth of this system (e.g., Cooper pairs in superconductors[69] and excitons in semiconductor quantum wells[70]). The measurement of the center frequency and line shape will require the acquisition of the full terahertz waveform, $E(t)$, in addition to the pump-probe data shown in Fig. 4(b).

Figure 4(c) data were taken under external photoexcitation at a delay of $\tau = 10$ ps after arrival of the pump pulse. These show the waveforms taken from $B_y = 5$ T to $B_y = 25$ T in $\Delta B_y = 2.5$ T increments as well as at $B_y = 0$ T.[71] We first acquired the full transmitted terahertz waveform without optical excitation ($\mathcal{U} = 0$) and then acquired a full terahertz waveform with $\mathcal{U} = 0.2$ mJ over the full 1 cm aperture

of the magnet ($\mathcal{F} = 0.25$ mJ cm^{-2}). The data presented in Fig. 4(c) are the difference between these two waveforms, $\Delta E_s(t) \equiv E_s(\mathcal{U}, t) - E_s(\mathcal{U} = 0, t)$. The use of direct subtraction as opposed to lock-in detection techniques was the result of the difficulty in operating the chopper needed within the fringing field of the Split-Helix magnet system. Finally, Fig. 4(d) shows the calculated Fourier transform, $\Delta\tilde{E}(\nu) = \mathrm{FT}[\Delta E_s(t)]$, of the data shown in Fig. 4(c), which shows the same narrowed bandwidth as was the case in Fig. 4(a) but with a variable phase that is a measure of the light-induced changes to the refractive index at each field.

Photoexcitation with an above the bandgap femtosecond pulse initially results in the creation of a population of nonthermal (i.e., "hot") electrons whose k-space distribution is determined by the center wavelength and bandwidth of the femtosecond pulse as well as the joint density of states and transition matrix element values between the valence and conduction sub-bands in gallium arsenide.[72] The system undergoes rapid thermalization on a $\tau \leq 0.3$ ps time scale (energy relaxation time) to establish quasi-Boltzmann distributions with separate temperatures for each sub-band.[73] Data acquired at a pump-probe delay of $\tau = 10$ ps, therefore, measure the system after thermalization of hot carriers is essentially completed. We note that Fig. 4(b) shows a more complicated set of temporal dynamics occurring within the first few picoseconds after photoexcitation when the system is far from equilibrium, which will be the focus of future work.
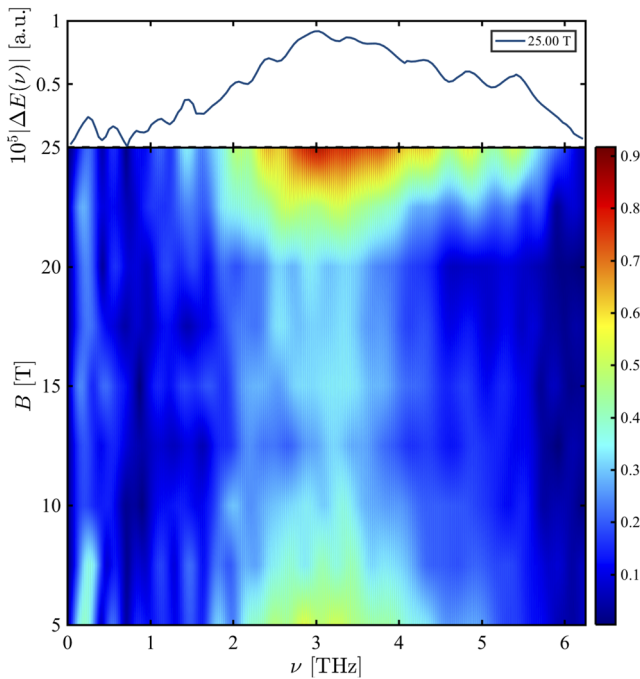
FIG. 5. The magnitude of numerical Fourier transforms of the change to the transmitted terahertz waveforms, $\Delta E(t)$, as a function of the magnetic field that were shown in the time-domain in Fig. 4(c). The top axis highlights one of the magnitudes at 25 T that is shown in the bottom figure. There exists a reduction in THz transmission as the field from 0 T until approximately $B_y = 15$ T, followed by an increase in the waveform transmission across this spectral range above this B_y. Application of an external parallel magnetic field is known to suppress inter-well tunneling above $B_y = 2.0$ T where the magnetic length, $\ell = 18$ nm, is equal to the well width,[65] as is discussed in further detail in the text of this paper. The origin of the *increase* in transmission above 17.5 T is currently unclear and will require further work.

Figure 5 shows the magnitude of the numerical Fourier transform of $\Delta E(t)$ as a function of both frequency and applied magnetic field, B. The suppression of $\Delta E_s(t)$ above 10 T is the result of the suppression of inter-well tunneling.[65] At $B = 0$ T, quantum tunneling between the four quantum wells is non-negligible, despite the relatively wide barrier layer (190 nm). Prior work has shown that this can be suppressed with an external B above a critical field corresponding to a magnetic length, $\ell = \frac{\hbar}{eB}$, that equals the quantum well width; this occurs for a 18 nm quantum well at fields ≥ 2 T. Suppression of inter-well scattering *reduces* dissipation and leads to an increase in the in-plane conductivity. Above this limit, there is a reduction in overall ΔE from an increase in in-plane conductivity for each individual well. This reduces the amplitude of the transmitted terahertz field, $E(t)$, and, thus, the photoinduced *change*, as well. We note that this reduction in $\Delta E_s(t)$ continues until 17.5 T, at which point the amplitude of ΔE again increases, implying a reduction in in-plane conductivity in these wells. Further experiments and computational modeling will be needed to explain this high field limit.

VI. CONCLUSIONS AND FUTURE DIRECTIONS

Our new instrument uses the Split Florida-Helix magnet system to study the terahertz frequency transmission of a doped multiple quantum well sample after photoexcitation by an above the bandgap femtosecond pulse. We generate ultrafast terahertz pulses that use nonlinear interactions in nitrogen and produce pulses with bandwidth from 0.3 to 10 THz. We demonstrate an optical pump terahertz probe spectrometer that resolves the changes to the terahertz frequency transmission of a multiquantum well sample that has been photo-excited at 800 nm. We find that the terahertz pulse after transmission through our sample has an upper frequency near 6.25 THz due to the well-known reststrahlen absorption in the constituent materials (i.e., GaAs, AlAs, and $Al_{0.24}Ga_{0.76}As$).

Future study with this instrument will resolve the open questions with the $\tau \leq 10$ ps data as well as using this instrument to study other materials with magnetic field dependent properties of interest. The study of correlated electronic materials like superconductors, other transition metal oxides, and heavy fermions on ultrafast time scales in a high magnetic field is a key driver of our experiment design. Further modification of this experiment will focus on two major design goals. As discussed above, the high electrical power requirements of this magnet necessitate the development of experimental capabilities that *rapidly* acquire the data in Fig. 4, where each data point in the sampled waveform was taken at a fixed t and the time resolution was achieved by varying the path length, d. A number of alternate detectors are used in terahertz time-domain spectroscopy that recover the terahertz waveform by rapidly scanning the delay stage,[74] employing an etalon to tilt the gate pulse,[49] or by chirping the gate pulse.[75] The second goal is to expand the instrument to both magnetic field geometries. The experiments shown in this manuscript have been exclusively in the Voigt (i.e., $\vec{k} \perp \vec{B}$ and referred to as B_y in this manuscript) geometry, but the development of a version that operates in the Faraday geometry (i.e., $\vec{k} \parallel \vec{B}$ and referred to as B_z in this manuscript) is a future goal of our collaboration.

[1] A. Paul, R. A. Bartels, R. Tobey, H. Green, S. Weiman, I. P. Christov, M. M. Murnane, H. C. Kapteyn, and S. Backus, Nature **421**, 51 (2003).

[2] S. Backus, C. G. Durfee, M. M. Murnane, and H. C. Kapteyn, Rev. Sci. Instrum. **69**, 1207 (1998).

[3] A. G. Čabo, J. A. Miwa, S. S. Grønborg, J. M. Riley, J. C. Johannsen, C. Cacho, O. Alexander, R. T. Chapman, E. Springate, M. Grioni, J. V. Lauritsen, P. D. C. King, P. Hofmann, and S. Ulstrup, Nano Lett. **15**, 5883 (2015).

[4] R. D. Averitt and A. J. Taylor, J. Phys.: Condens. Matter **14**, R1357 (2002).

[5] D. Fausti, R. I. Tobey, N. Dean, S. Kaiser, A. Dienst, M. C. Hoffmann, S. Pyon, T. Takayama, H. Takagi, and A. Cavalleri, Science **331**, 189 (2011).

[6] J. Zhang, X. Tan, M. Liu, S. W. Teitelbaum, K. W. Post, F. Jin, K. A. Nelson, D. N. Basov, W. Wu, and R. D. Averitt, Nat. Mater. **15**, 956 (2016).

[7] K. Nasu, in *Photoinduced Phase Transitions*, edited by K. Nasu (World Scientific Pub. Co., Inc., 2004).

[8] M. P. Lilly, K. B. Cooper, J. P. Eisenstein, L. N. Pfeiffer, and K. W. West, Phys. Rev. Lett. **82**, 394 (1999).

[9] E. Fradkin and S. A. Kivelson, Phys. Rev. B **59**, 8065 (1999).

[10] E. Fradkin, S. A. Kivelson, E. Manousakis, and K. Nho, Phys. Rev. Lett. **84**, 1982 (2000).

[11] T. Arikawa, K. Hyodo, Y. Kadoya, and K. Tanaka, Nat. Phys. **13**, 688 (2017).

[12] S. A. McGill, R. I. Miller, O. N. Torrens, A. Mamchik, I.-W. Chen, and J. M. Kikkawa, Phys. Rev. Lett. **93**, 047402 (2003).

[13] S. McGill, R. Miller, O. Torrens, A. Mamchik, I.-W. Chen, and J. Kikkawa, Phys. Rev. B **71**, 075117 (2005).

[14] D. N. Basov, R. D. Averitt, D. van der Marel, M. Dressel, and K. Haule, Rev. Mod. Phys. **83**, 471 (2011).

[15] V. Kabanov, J. Demsar, B. Podobnik, and D. Mihailovic, Phys. Rev. B **59**, 1497 (1999).

[16] G. Coslovich, B. Huber, W. S. Lee, Y. D. Chuang, Y. Zhu, T. Sasagawa, Z. Hussain, H. A. Bechtel, M. C. Martin, Z. X. Shen, R. W. Schoenlein, and R. A. Kaindl, Nat. Commun. **4**, 2643 (2013).

[17] L. Zhao, D. H. Torchinsky, H. Chu, V. Ivanov, R. Lifshitz, R. Flint, T. Qi, G. Cao, and D. Hsieh, Nat. Phys. **12**, 32 (2015).

[18] O. Krupin, G. L. Dakovski, B. J. Kim, J. W. Kim, J. Kim, S. Mishra, Y.-D. Chuang, C. R. Serrao, W. S. Lee, W. F. Schlotter, M. P. Minitti, D. Zhu, D. Fritz, M. Chollet, R. Ramesh, S. L. Molodtsov, and J. J. Turner, J. Phys.: Condens. Matter **28**, 32LT01 (2016).

[19] D. J. Hilton, R. P. Prasankumar, S. Fourmaux, A. Cavalleri, D. Brassard, M. A. E. Khakani, J. C. Keiffer, A. J. Taylor, and R. D. Averitt, Phys. Rev. Lett. **99**, 226401 (2007).

[20] P. Dey, J. Paul, Z. Wang, C. E. Stevens, C. Liu, A. H. Romero, J. Shan, D. J. Hilton, and D. Karaiskaj, Phys. Rev. Lett. **116**, 127402 (2016).

[21] J. Paglione and R. L. Greene, Nat. Phys. **6**, 645 (2010).

[22] J. J. Baumberg, D. D. Awschalom, N. Samarth, H. Luo, and J. K. Furdyna, Phys. Rev. Lett. **72**, 717 (1994).

[23] W. Li, C. L. Vicente, J. S. Xia, W. Pan, D. C. Tsui, L. N. Pfeiffer, and K. W. West, Phys. Rev. Lett. **102**, 216801 (2009).

[24] A. T. Hatke, M. A. Zudov, L. N. Pfeiffer, and K. W. West, Phys. Rev. B **85**, 241305 (2012).

[25] Q. Shi, M. A. Zudov, J. D. Watson, G. C. Gardner, and M. J. Manfra, Phys. Rev. B **93**, 121404 (2016).

[26] M. A. Zudov, R. R. Du, J. A. Simmons, and J. L. Reno, Phys. Rev. B **64**, 201311(R) (2001).

[27] R. A. Kaindl, D. Hägele, M. A. Carnahan, and D. S. Chemla, Phys. Rev. B **79**, 045320 (2009).

[28] X. Wang, D. J. Hilton, L. Ren, D. M. Mittleman, J. Kono, and J. L. Reno, Opt. Lett. **32**, 1845 (2007).

[29] J. A. Curtis, T. Tokumoto, A. T. Hatke, J. G. Cherian, J. L. Reno, S. A. McGill, D. Karaiskaj, and D. J. Hilton, Phys. Rev. B **93**, 155437 (2016).

[30] J. A. Curtis, T. Tokumoto, N. K. Nolan, L. M. McClintock, J. G. Cherian, S. A. McGill, and D. J. Hilton, Opt. Lett. **39**, 5772 (2014).

[31] R. Laughlin, Phys. Rev. B **23**, 5632 (1981).

[32] R. Laughlin, Phys. Rev. Lett. **50**, 1395 (1983).

[33] G. S. Boebinger, A. Passner, L. N. Pfeiffer, and K. W. West, Phys. Rev. B **43**, 12673 (1991).

[34] H. J. Gardner, A. Kumar, L. Yu, and P. Xiong, Nat. Phys. **7**, 895 (2011).

[35] R. D. Averitt, A. I. Lobad, C. Kwon, S. A. Trugman, V. K. Thorsmølle, and A. J. Taylor, Phys. Rev. Lett. **87**, 017401 (2001).

[36] J. Lloyd-Hughes, H. E. Beere, D. A. Ritchie, and M. B. Johnston, Phys. Rev. B **77**, 125322 (2008).

[37] F. Bitter, Rev. Sci. Instrum. **10**, 373 (1939).

[38] S. Crooker, Rev. Sci. Instrum. **73**, 3258 (2002).

[39] S. Zaric, G. N. Ostojic, J. Kono, J. Shaver, V. C. Moore, M. S. Strano, R. H. Hauge, R. E. Smalley, and X. Wei, Science **304**, 1129 (2004).

[40] L. Yang, N. A. Sinitsyn, W. Chen, J. Yuan, J. Zhang, J. Lou, and S. A. Crooker, Nat. Phys. **11**, 830 (2015).

[41] K. Wang and D. M. Mittleman, Nature **432**, 376 (2004).

[42] M. Furis, J. A. Hollingsworth, V. I. Klimov, and S. A. Crooker, J. Phys. Chem. B **109**, 15332 (2005).

[43] D. Mittleman, *Sensing with Terahertz Radiation* (Springer, 2002).

[44] M. Tonouchi, Nat. Photonics **1**, 97 (2007).

[45] U. Nagel, R. S. Fishman, T. Katuwal, H. Engelkamp, D. Talbayev, H. T. Yi, S.-W. Cheong, and T. Rõõm, Phys. Rev. Lett. **110**, 257201 (2013).

[46] D. Szaller, V. Kocsis, S. Bordács, T. Fehér, T. Rõõm, U. Nagel, H. Engelkamp, K. Ohgushi, and I. Kézsmárki, Phys. Rev. B **95**, 024427 (2017).

[47] S. Yu, B. Gao, J. W. Kim, S.-W. Cheong, M. K. L. Man, J. Madéo, K. M. Dani, and D. Talbayev, Phys. Rev. Lett. **120**, 037601 (2018).

[48] G. T. Noe II, H. Nojiri, J. Lee, G. L. Woods, J. Léotin, and J. Kono, Rev. Sci. Instrum. **84**, 123906 (2013).

[49] G. T. Noe, I. Katayama, F. Katsutani, J. J. Allred, J. A. Horowitz, D. M. Sullivan, Q. Zhang, F. Sekiguchi, G. L. Woods, M. C. Hoffmann, H. Nojiri, J. Takeda, and J. Kono, Opt. Express **24**, 30328 (2016).

[50] M. Bird, S. Bole, and S. R. Gundlach, U.S. patent application 11/716,492 (March 9, 2007).

[51] K.-Y. Kim, A. J. Taylor, J. H. Glownia, and G. Rodriguez, Nat. Photonics **2**, 605 (2008).

[52] J. Toth, M. D. Bird, S. Bole, and J. W. O'Reilly, IEEE Trans. Appl. Supercond. **22**, 4301604 (2012).

[53] Z. Wang, J. Shan, and K. F. Mak, Nat. Nanotechnol. **12**, 144 (2016).

[54] M. Kress, T. Löffler, S. Eden, M. Thomson, and H. G. Roskos, Opt. Lett. **29**, 1120 (2004).

[55] N. Karpowicz, X. Lu, and X. C. Zhang, J. Mod. Opt. **56**, 1137 (2009).

[56] X. Lu, N. Karpowicz, and X.-C. Zhang, J. Opt. Soc. Am. B **26**, A66 (2009).

[57] R. T. Hall, J. Chem. Phys. **47**, 2454 (1967).

[58] J. W. Goodman, *Introduction to Fourier Optics*, 2nd ed. (McGraw-Hill Science/Engineering/Math, 1996).

[59] This was approximately 30 minutes per each waveform at each B_y for the data shown in Fig. 4.

[60] C. Schmuttenmaer, Chem. Rev. **104**, 1759 (2004).

[61] A. Gürtler, C. Winnewisser, H. Helm, and P. U. Jepsen, J. Opt. Soc. Am. A **17**, 74 (2000).

[62] X. Wang, D. J. Hilton, J. L. Reno, D. M. Mittleman, and J. Kono, Opt. Express **18**, 12354 (2010).

[63] T. Maag, A. Bayer, S. Baierl, M. Hohenleutner, T. Korn, C. Schüller, D. Schuh, D. Bougeard, C. Lange, R. Huber, M. Mootz, J. E. Sipe, S. W. Koch, and M. Kira, Nat. Phys. **12**, 119 (2015).

[64] C. J. Dorow, M. W. Hasling, E. V. Calman, L. V. Butov, J. Wilkes, K. L. Campman, and A. C. Gossard, Phys. Rev. B **95**, 235308 (2017).

[65] G. Gumbs, Phys. Rev. B **54**, 11354 (1996).

[66] S. Adachi, J. Appl. Phys. **58**, R1 (1985).

[67] J. S. Gaffney, N. A. Marley, and D. E. Jones, in *Characterization of Materials*, edited by E. N. Kaufmann (John Wiley and Sons, Inc., Hoboken, NJ, USA, 2002), pp. 1–33.

[68] Data at 25 T were not taken here to conserve the limited electrical power for future experiments.

[69] J. Demsar, R. Averitt, A. J. Taylor, and V. Kabanov, Phys. Rev. Lett. **91**, 267002 (2003).

[70] D. Karaiskaj, A. D. Bristow, L. Yang, X. Dai, R. P. Mirin, S. Mukamel, and S. T. Cundiff, Phys. Rev. Lett. **104**, 117401 (2010).

[71] The data point at B_y = 2.5 T is absent since we did not have the needed time to acquire an additional data set, which we discuss in greater detail in Sec. IV E of this manuscript.

[72] D. J. Hilton, in *Optical Techniques for Solid-State Materials Characterization*, edited by R. P. Prasankumar and A. J. Taylor (CRC Press, Boca Raton, 2011), pp. 329–370.

[73] F. Ganikhanov, K. C. Burr, D. J. Hilton, and C. L. Tang, Phys. Rev. B **60**, 8890 (1999).

[74] F. Tauser, C. Rausch, J. H. Posthumus, and F. Lison, Proc. SPIE **6881**, 68810O (2008).

[75] B. Yellampalle, K. Y. Kim, G. Rodriguez, J. H. Glownia, and A. J. Taylor, Appl. Phys. Lett. **87**, 211109 (2005).